NUCLEAR REACTIONS -- THEORY

Time-Dependent Hartree-Fock-Bogoliubov Approximation and the Nonintegrable Quantum Phase

Aurel Bulgac

It is commonly believed that to describe any type of collective motion, one needs potential and kinetic energy terms only. However, it can be shown[1] that effective gauge fields must be considered when constructing effective hamiltonians for different types of collective motion. They correspond to vector type of potentials, which have never been considered in any collective model.

The sources of such effective gauge fields are different degeneracies or level crossings in the single-particle spectra, through a mechanism put in evidence by Berry (the so-called Berry's phase). In the collective manifold at these points, one finds effective magnetic charges, Dirac monopoles. The presence of such effective gauge fields modifies the quantization rules for the collective wave functions and leads to the appearance of a new type of force, which depends on the collective velocity.

In the framework of ATDHFB (adiabatic time-dependent Hartree-Fock-Bogoliubov equations) one can derive an effective hamiltonian for the collective motion of the pairing field. We show explicitly[2] how the effective gauge potentials appear in such a case. As a by-product, we point to an inaccuracy in the formulation of the TDHFB equations of motion. Moreover, the requantization of the collective motion leads to expected correct results only when the effective gauge field is actually taken into account.

References

1. A. Bulgac, Phys. Rev. A37, 4048 (1988).

2. A. Bulgac, preprint MSUCL-665, October 1988, submitted for publication.

Cutting Rules in Many-Body Theory

Pawel Danielewicz

The high-order structure of diagrammatic expansion in real-time many-body theory has been examined[1]. The existence of cutting rules has been demonstrated for diagrams that represent the production and absorption rates in the medium. The rules permit one to express the rates as the convolutions of retarded amplitudes with the densities in the system, and allow for an expansion in the number of interacting bodies. This extends the S-matrix theory to the situation where more than two bodies collide and also when the bodies are medium excitations. As an example of the application of the rules, a resummation has been carried over repeated interactions of particles and holes[1] for the single-particle production and absorption rates. Further, the formulae for the absorption and production rates of collective excitations were derived.

The results can be further used in transport theory of nuclear collisions for treating subthreshold production, involving several nucleons, absorption involving several bodies, and light fragment production. Appropriate relativistic modifications in the theory can be found in Refs. 2 and 3. Current efforts concentrate on subthreshold antiproton production, backward proton production, and the deuteron production.

References

1. P. Danielewicz, "Operator Expectation Values, Self-Energies, Cutting Rules, and Higher-Order Processes in Quantum Many-Body Theory," Report MSUCL-691, accepted for Annals of Physics.

2. St. Mrowczynski and P. Danielewicz, "Green Function Approach to Transport Theory of Scalar Fields," U. of Regensburg Report.

3. W. Botermans and R. Malfliet, Phys. Lett. B 215, 617 (1988).

Configurational Quasidegeneracy and the Liquid Drop Model

Aurel Bulgac

Zamick *et al.*[1] recently reported on a series of Hartree-Fock calculations of light nuclei with Skyrme interaction in which they observed a near degeneracy of states corresponding to different fillings of the single-particle levels for different light nuclei. The question they addressed was: What excitation energies correspond to such states as 2p-2h, 4p-4h, ..., 8p-8h? When exciting a number of particles from the ground state, the nucleus loses its sphericity.

A long time ago, Hill and Wheeler[2] remarked that there must be a relatively simple relation between the number of excited particle-hole pairs and the intrinsic deformation of a nucleus. Bertsch[3] derived a very simple formula, which links these two quantities. One might expect that the main trend of the deformation energy, obtained in a Hartree-Fock calculation, must be fairly well described by the liquid drop model, if one had a way to predict the intrinsic deformation, corresponding to the excitation of a given number of particle-hole pairs.

Using the liquid drop model stiffness[4] and the relation between the deformation and the number of particle-hole pairs from Ref. 3, we were able to predict[5] rather accurately the results of the Hartree-Fock calculations, reported in Ref. 1. The remaining discrepancies can be attributed to pairing correlations and shell corrections, obviously absent in a drop model approach. However, the significant lowering of the excitation energies of the states (corresponding to a rather large number of ph-pairs) can be understood in this way quite easily.

References

1. H. Liu and L. Zamick, Phys. Rev. C29, 1040 (1984); H. Liu, L. Zamick and H. Jaqaman, Phys. Rev. C31, 2251 (1985); D.C. Zheng, D. Berdichevsky and L. Zamick, Phys. Rev. C38, 437 (1988).

2. D.L. Hill and J.A. Wheeler, Phys. Rev. 89, 1102 (1953).

3. G.F. Bertsch, Phys. Lett. 95B, 157 (1980).

4. W.D. Myers and W.J. Swiatecki, Nucl. Phys. 81, 1 (1966).

5. A. Bulgac, preprint MSUCL-660, October 1988, published Phys. Rev. C40, 1073 (1989).

Pion Production in Heavy-Ion Collisions

Wolfgang Bauer

In nucleon-nucleon collisions, pions can only be produced if the incoming proton has a kinetic energy $E_{kin} > E_{thr} = 2M_\pi + M_\pi^2/2M_N \approx 290$ MeV. However, in nucleus-nucleus collisions, one finds that pions are produced at beam energies per nucleon well below E_{thr}. It is the main goal of studying pion production in nucleus-nucleus collisions at sub-threshold energies to find out if these pions are produced collectively by many nuclei pooling their energy, or if the pions are predominantly produced in individual incoherent nucleon-nucleon collisions during the course of the reaction.

For both production pictures, models have been forwarded. Both classes of models are able to fit total pion production cross sections in light systems quite well. To distinguish between the different production mechanisms, we have studied the mass dependence of the total production cross section and also the pion energy spectra.

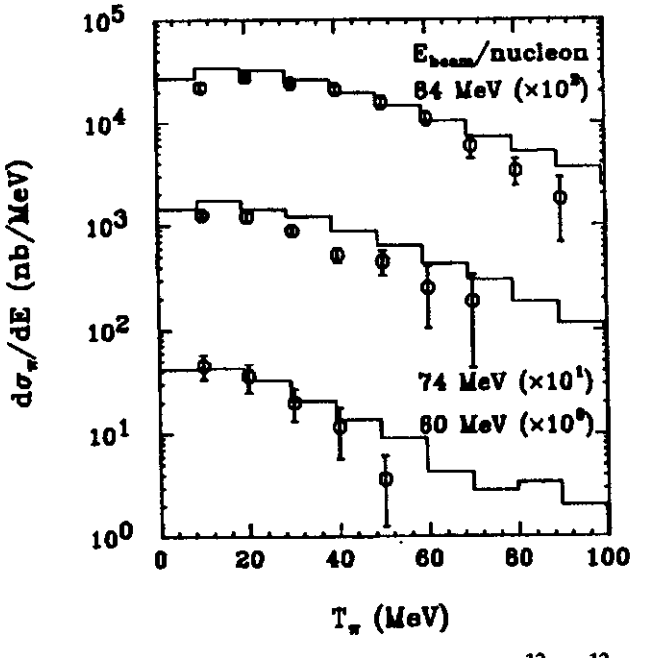

FIG. 1: Energy spectra of neutral pions from collisions of ^{12}C + ^{12}C at beam energies per nucleon of 60, 74, and 84 MeV. The histograms represent the data and are taken from Ref. 4. The plot symbols with statistical error bars are the result of our calculations.

We have forwarded a model based on a picture of pion production via individual nucleon-nucleon collisions[1]. The energies and momenta of the pion-producing nucleons are calculated via the numerical solution of the Boltzmann-Uehling-Uhlenbeck equation[2]. The differential pion production cross section is calculated via

$$\sigma_\pi = \int db^2 \sum_{coll(b)} \int \frac{d\Omega''}{4\pi} \pounds P_\pi(p_1,p_2)(1-\bar{f}(r,p_4,t)) X_{abs}(A).$$

$P_\pi = \sigma_\pi/\sigma_{tot}$ is the pion production probability for two nucleons having momenta p_1 and p_2, and it is parameterized using experimental free nucleon-nucleon cross sections. The final state momenta p_3 and p_4 of the two nucleons are related to the initial state momenta and the pion momentum by energy and momentum conservation. The integration over $d\Omega$ is over the two degrees of freedom (the pair of relative angles between initial and final state momenta) which are not determined by these conservation laws. £ represents a Lorentz transformation from the nucleon-nucleon center of mass system to the system of calculation. Pion reabsorption is taken into account via a phenomenological mass-dependent factor $X_{abs}(A)$. In determining the production kinematics, we assume that the dominant channel for the pion production is $N+N \rightarrow N+\Delta \rightarrow N+N+\pi$. For the mass distribution of the Δ we use the parameterization of Kitazoe *et al.*[3]

In Fig. 1, we show a comparison of the energy spectra of neutral pions from collisions of ^{12}C + ^{12}C at various beam energies. The results of the calculations are represented by the plot symbols, and the histograms represent the data of Noll *et al.*[4] Even though our calculations show slightly steeper energy spectra than the data, one can say that there is good agreement between experiment and the theory which is based on an individual nucleon-nucleon pion production picture.

However, it is important to perform the calculations with a very good dynamical description of the colliding nuclear system. Using the identical production mechanism but combined with a simple Fermi gas model, we found that the data in this approach are underpredicted by almost an order of magnitude[1].

Collective production models predict a dependence of the total pion production probability proportional to the square of the "charge", in this case the baryon number in the subthreshold region. A nucleon-nucleon production picture should only carry a linear dependence on the baryon number. There are effects of the reaction geometry and reabsorption that obscure this simple signature, but this is the basic motivation with which studies on the mass and beam-energy dependence of the pion production were carried out[5]. By taking the ratio of production cross section of pions from heavy-ion systems of different mass, one should be able to obtain hints on the degree of collectivity involved in the production process. A change in this ratio as the beam energy sinks below the threshold value could then be a possible signature for collectivity.

In Fig. 2, we compare our calculations for the total production cross section for negative pions to the experimental data[5] for beam energies per nucleon between 100 and 800 MeV. For both systems (light and heavy), the theory based on a nucleon-nucleon production picture reproduces the data (with the exception of the Ne + NaF data point at 183 MeV/nucleon) accurately. Since we also are able to match the excitation function for the C + C system for beam

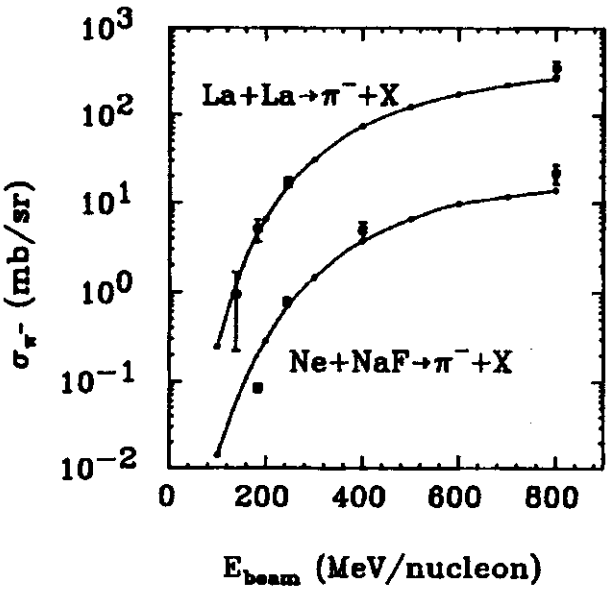

FIG. 2: Production cross sections for π^- emitted at $\theta_{c.m.} = 90°$. The solid curves represent the theoretical calculations, and the plot symbols with error bars are the experimental data of Ref. 5.

energies of 60, 74, and 84 MeV/nucleon, we conclude that the dominant production process for subthreshold pions in heavy-ion collisions is the incoherent superposition of individual nucleon-nucleon production processes. There is no need for an additional collective contribution to explain the available data.

References

1. W. Bauer, Phys. Rev. C 40, 494 (1989); W. Bauer, Preprint MSUCL-699.

2. G.F. Bertsch and S. Das Gupta, Phys. Rep. 160, 189 (1988).

3. Y. Kitazoe *et al.*, Phys. Lett. 166B, 35 (1986).

4. H. Noll *et al.*, Phys. Rev. Lett. 52, 1284 (1984).

5. J. Miller *et al.*, Phys. Rev. Lett. 59, 519 (1987).

Nuclear Stopping at Intermediate Beam Energies

Wolfgang Bauer

It is expected that one can extract information on the nuclear compressibility from nuclear collective motion in heavy ion collisions. At present, however, the standard techniques of measuring the nuclear "flow" have not yielded precise answers. To this end, we have proposed a way of looking at nuclear collective stopping instead of nuclear collective deflection. This is achieved by constructing the quadrupole moment tensor of the nucleon momentum distribution

$$Q_{\alpha\beta} = \int d\vec{p}(3p_\alpha p_\beta - p^2\delta_{\alpha\beta})\rho(\vec{p}) = \sum_{i=1}^{A_T+A_P}(3(\vec{p}_i)_\alpha(\vec{p}_i)_\beta - p_i^2\delta_{\alpha\beta}).$$

In principle, the same information about nuclear stopping could also be extracted from, for example, dN/dy distributions or double differential cross sections. However, it is desirable to possess a measure that characterizes the degree of nuclear stopping by one number. The diagonal element along the beam axis of the above tensor, Q_{zz}, provides such information. For a completely equilibrated system, its value is 0, and two noninteracting Fermi gases have a value of

$$Q_{zz}^{FG} = 4Ap_b^2,$$

where p_b is the beam momentum in the center-of-mass system and $A = A_T = A_P$ is the mass number of projectile and target.

We have studied Q_{zz} for symmetric heavy ion systems as a function of the impact parameter, incident energy, and mass number in model simulations based on the numerical solution of the Boltzmann-Uehling-Uhlenbeck transport equation[1]. From the model simulations, Q_{zz} can be extracted via

$$Q_{zz} = \lim_{t\to\infty}\int\frac{d\vec{x}d\vec{p}}{(2\pi)^3}(2p_z^2 - p_x^2 - p_y^2)f(\vec{r},\vec{p},t),$$

where $f(\vec{r},\vec{p},t)$ is the phase space distribution function of the test particles.

We find a strong dependence of Q_{zz} on the impact parameter, thus establishing this observable as a possible centrality trigger. We also predict that Q_{zz} increases almost linearly with beam energy above a mass-dependent threshold value. For a given beam energy, Q_{zz} decreases with projectile and target mass number. Based on the results of our calculations, we predict that even at a beam energy of 100 MeV/nucleon, nuclei can completely stop each other in central collisions, provided that $A_T = A_P > 150$.

Comparing our numerical results to analytical scaling functions, we predict that the mass dependence of Q_{zz} can be used to extract the value of the nuclear compressibility from comparison of the results of different model assumptions with experimental data.

References

1. W. Bauer, Phys. Rev. Lett. 61, 2534 (1988).

Mass Fluctuation in Time-Dependent Density-Matrix Formalism

M. Gong and M. Tohyama

One of characteristic aspects of the deep-inelastic heavy-ion collisions (DIC) is broad distributions of observables such as mass, charge, energy and momentum. The most fundamental theory so far applied to DIC is the time-dependent Hartree-Fock theory (TDHF). Although the mean values of one-body observables in DIC are reproduced in TDHF, their fluctuations predicted in TDHF were found to be quite small[1]. This difficulty is due to the one-body nature of TDHF: the total wave function in TDHF is restricted to a single Slater determinant.

We studied the mass fluctuations in DIC, using an extended TDHF theory which includes the effects of nucleon-nucleon collisions. This theory which we call the time-dependent density matrix theory (TDDM) is derived from a density-matrix formalism given by Wang and Cassing[2]. The advantage of TDDM is that it provides us with a two-body density matrix which is necessary to calculate the fluctuations of one-body quantities. TDDM consists of three coupled equations. The first equation is for the single-particle states,

$$i\hbar\dot{\psi}_\lambda(1,t)=\left[-\hbar^2\frac{\nabla^2}{2M}+U[\rho]\right]\psi_\lambda(1,t), \tag{1}$$

where $U[\rho]$ is the mean field. The second equation is for the occupation matrix $n_{\alpha\beta}$,

$$i\hbar\dot{n}_{\alpha\beta}=\sum_{\gamma\delta\sigma}\{C_{\gamma\delta\beta\sigma}<\alpha\sigma|v|\gamma\delta>-C_{\alpha\delta\gamma\sigma}<\gamma\sigma|v|\beta\delta>\}, \tag{2}$$

where C is a two-body density matrix and v is a two-body interaction. The equation of motion for C contains a first-order particle-particle interaction term (Born term), higher-order particle-hole and particle-particle correlation terms,

$$i\hbar\dot{C}_{\alpha\beta\alpha'\beta'}=\sum_{\lambda_1\lambda_2\lambda_3\lambda_4}<\lambda_1\lambda_2|v|\lambda_3\lambda_4>A\{(\delta_{\alpha\lambda_1}-n_{\alpha\lambda_1})(\delta_{\beta\lambda_2}-n_{\beta\lambda_2})n_{\lambda_3\alpha'}n_{\lambda_4\beta'}$$
$$n_{\alpha\lambda_1}n_{\beta\lambda_2}(\delta_{\lambda_3\alpha'}-n_{\lambda_3\alpha'})(\delta_{\lambda_4\beta'}-n_{\lambda_4\beta'})\}$$
$$+\text{ higher order terms} \tag{3}$$

where the first term on the right-hand side is the Born term. The full expression for the higher-order terms are shown in Ref. 3. These coupled equations satisfy conservation laws of total number of particles, total momentum and energy.

In DIC there are two fragments in the final state of a collision. To count the number of nucleons in one of the fragments, we introduce a number operator[1]

$$N_R=\int_R d\vec{r}\,a^\dagger(\vec{r})a(\vec{r}). \tag{4}$$

where $a^\dagger(\vec{r})$ and $a(\vec{r})$ are the creation and annihilation operators, respectively, and the subscript R means that the integration is restricted to half space containing one of the two fragments. The dispersion σ_R of the mass distribution is given by

$$\sigma_R^2 = \langle N_R^2 \rangle - \langle N_R \rangle^2$$

$$= \sum_{\alpha\beta} n_{\alpha\beta} \langle \beta | \alpha \rangle_R + \sum_{\alpha\beta\alpha'\beta'} \langle \alpha' | \alpha \rangle_r \langle \beta' | \beta \rangle_r (C_{\alpha\beta\alpha'\beta'} - n_{\alpha\beta\alpha'\beta'}), \quad (5)$$

where $\langle \alpha | \beta \rangle_R$ is the overlap integral of the two single-particle states α and β in the half space. Since the total system is an eigenstate of the total number operator, the dispersion for the entire space must be zero:

$$\sigma^2_{\text{total}} = \sum_{\alpha} n_{\alpha\alpha} + \sum_{\alpha\beta} (C_{\alpha\beta\alpha\beta} - n_{\alpha\beta} n_{\beta\alpha} = A + \sum_{\alpha\beta} (C_{\alpha\beta\alpha\beta} - n_{\alpha\beta} n_{\beta\alpha}) = 0 \quad (6)$$

where $\langle \alpha | \beta \rangle_{\text{total}} = \delta_{\alpha\beta}$ is used. In order to satisfy this condition, we have to keep all the higher-order terms in Eq. (3).

We apply TDDM to $^{16}O + ^{16}O$ at E_{lab} = 185 MeV. The single-particle wave functions are calculated with the TDHF code described in Ref. 4. Eqs. 2 and 3 are solved with the Runge-Kutta method. The residual interaction is taken to be a δ function $v = v_0 \delta^3(r\text{-}r')$ with v_0 = -300 MeV fm^3. Since there is no available data for $^{16}O + ^{16}O$, we compare our results with those calculated in a transport model called nucleon exchange transport model (NET)[5]. We determined macroscopic parameters of NET based on the results of TDDM calculations. The mass dispersions are given in Table I. The TDDM mass dispersions are much larger than the TDHF ones and comparable to the NET results. Since the NET values are considered "empirical", the mass fluctuations in TDDM may be large enough to reproduce experimental data.

TABLE I: σ_A calculated in TDDM, TDHF and NET for a head-on collision and a peripheral collision of $^{16}O + ^{16}O$ at E_{lab} = 185 MeV.

	σ_A (amu)	
Theory	$l = 0\hbar$	$l = 40\hbar$
TDDM	2.0	1.2
TDHF	0.8	0.4
NET	2.7	1.5

References

1. K.T.R. Davies, K.R.S. Devi, S.E. Koonin and M.R.Strayer, *Treaties on Heavy Ion Science*, III (Plenum, New York, 1985).

2. S.J. Wang and W. Cassing, Ann. Phys. 159, 328 (1985).

3. M. Gong and M. Tohyama, submitted to Z. Phys.

4. K.T.R. Davies and S.E. Koonin, Phys. Rev. C23, 2042 (1981).

5. J. Randrup, Nucl. Phys. A307, 319 (1978).

Small Amplitude Limit of Time-Dependent Density Matrix Theory

M. Tohyama and M. Gong

Much work has been done on the derivation of the extended time-dependent Hartree-Fock theory (ETDHF) which incorporates the effects of two-body collisions[1]. To get a better understanding of ETDHHF, it is useful to investigate ETDHF in various limits and compare them with existing theories. Here we discuss the small amplitude limit of one of ETDHF's, i.e., the time-dependent density matrix theory (TDDM.)

TDDM, which has been proposed by Wang and Cassing[2], determines the time evolution of a one-body density matrix ρ and a two-body correlation function C_2. In the small amplitude limit of TDDM, ρ and C_2 are expanded around ground-state values ρ_0 and C_{20} as:

$$\begin{aligned} \rho(11';t) &= \rho_0(11') + \delta\rho(11';t) \\ C_2(121'2';t) &= C_{20}(12,1'2') \\ &\quad + \delta C_2(121'2';t), \end{aligned} \tag{1}$$

and the equations of motion for ρ and C_2 are linearized with respect to $\delta\rho$ and δC_2. We expand $\delta\rho$ and δC_2 in terms of the eigenstates of a mean-field hamiltonian $\{\psi_\alpha\}$. The expansion coefficient $n_{\alpha\beta}$ of $\delta\rho$, which is called the one-body amplitude, satisfies:

$$\begin{aligned} (\omega - \epsilon_\alpha + \epsilon_\beta) n_{\alpha\beta} &= \sum_{\alpha'\beta'\gamma} \{ <\gamma\beta'|v|\alpha'\beta>_A n^0_{\alpha\gamma} - <\alpha\beta'|v|\alpha'\gamma>_A n^0_{\gamma\beta} \} n_{\alpha'\beta'} \\ &\quad + \sum_{\beta'\gamma\delta} \{ <\alpha\beta'|v|\gamma\delta> C_{\gamma\delta\beta\beta'} - <\gamma\beta'|v|\beta\delta> C_{\alpha\delta\gamma\beta'} \}, \end{aligned} \tag{2}$$

where $m^0_{\alpha\beta}$ is the ground-state occupation matrix and $C_{\alpha\beta\gamma\delta}$ is the expansion coefficient of δC_2, i.e. the two-body amplitude. The equation for the two-body amplitude is

$$(\omega - \epsilon_\alpha - \epsilon_\beta + \epsilon_{\alpha'} + \epsilon_{\beta'}) C_{\alpha\beta\alpha'\beta'} = A_{\alpha\beta\alpha'\beta'} + B_{\alpha\beta\alpha'\beta'} + P_{\alpha\beta\alpha'\beta'} + H_{\alpha\beta\alpha'\beta'}, \tag{3}$$

where *A, B, P,* and *H* come from the linearization of the mean field hamiltonian, the Born term, higher-order particle-particle correlation terms and higher-order particle-hole terms, respectively. The full expression for *A, B, P,* and *H* is given in Ref. 3. Equations (2) and (3) are the basic equations in the small amplitude limit of TDDM (STDDM).

In the following, we discuss STDDM in limiting cases. For simplicity, we assume that the HF ground state is a good approximation for the true ground state. This means that $n^0_{\alpha\beta} = \delta_{\alpha\beta}(= 0)$ for occupied (unoccupied) states.

1. Random phase approximation

If all the two-body amplitudes $C_{\alpha\beta\alpha'\beta'}$ are neglected, Eq.(2) is equivalent to the RPA equation for 1 particle (p) - 1 hole (h) amplitudes.

2. Second RPA

If we keep only the 1p-1h amplitudes ($X_1 = n_{pv}$ and $Y_1 = n_{vp}$) and the 2p-2h amplitudes ($X_2 = C_{pp'vv'}$ and $Y_2 = C_{vv'pp'}$), STDDM is equivalent to the second RPA of Sawicki[4]. The equations for the one-body and two-body amplitudes can be written in the matrix form[5],

$$\begin{vmatrix} A_{11} & B_{11}^{*} & A_{12} & O^{*} \\ -B_{11} & -A_{11}^{*} & O & -A_{12}^{*} \\ A_{21} & O^{*} & C_{22} & O^{*} \\ O & -A_{21}^{*} & O & -C_{22}^{*} \end{vmatrix} \begin{vmatrix} X_1 \\ Y_1 \\ X_2 \\ Y_2 \end{vmatrix} = \omega \begin{vmatrix} X_1 \\ Y_1 \\ X_2 \\ Y_2 \end{vmatrix}$$

where A_{11} and B_{11} are the RPA matrices,

$$A_{12} = A_{\rho\nu,\sigma'\mu'} = \langle\rho\mu'|v|\sigma\sigma'\rangle\delta_{\nu\mu} + \langle\mu\mu'|v|\sigma'\nu\rangle\delta_{\rho\sigma},$$

$$A_{21} = A_{\rho\rho'\nu\nu',\sigma\mu}$$
$$= \langle\rho\rho'|v|\sigma\nu'\rangle_A\delta_{\nu\mu} + \langle\rho\rho'|v|\nu\sigma\rangle_A\delta_{\mu\nu'}$$
$$+ \langle\rho\mu|v|\nu'\nu\rangle_A\delta_{\sigma\rho'} + \langle\rho\mu|v|\nu\nu'\rangle_A\delta_{\rho\sigma},$$

and

$$C_{22} = C_{\rho\rho'\nu\nu',\sigma\sigma'\mu\mu'} =$$
$$= (\epsilon_\rho + \epsilon_{\rho'} - \epsilon_\nu - \epsilon_{\nu'})\delta_{\rho\sigma}\delta_{\rho'\sigma'}\delta_{\nu\mu}\delta_{\nu'\mu'}$$
$$+ \langle\rho\rho p|v|\sigma\sigma'\rangle\delta_{\nu\mu}\delta_{\nu'\mu'}$$
$$+ \langle\rho\mu|v|\nu\sigma\rangle_A\delta_{\nu'\mu'}\delta_{\sigma'\rho'}$$
$$+ \langle\mu'\rho'|v|\sigma'\nu'\rangle_A\delta_{\mu\nu}\delta_{\sigma\rho}$$
$$+ \langle\rho\mu'|v|\nu'\sigma\rangle_A\delta_{\sigma'\rho'}\delta_{\mu\nu}$$
$$+ \langle\mu\rho'|v|\sigma'\nu\rangle_A\delta_{\rho\sigma}\delta_{\mu'\nu'}.$$

If the interaction terms in C_{22} are neglected, the aforementioned SRPA reduces to the SRPA discussed by Yannouleas *et al.*[6]. The neglect of the interaction in C_{22} corresponds to the Born approximation for C_2. The small amplitude limit of this SRPA was studied by Ayik and Dworzecka[7].

The small amplitude limit of TDDM is a generalization fo the second RPA of Sawicki[4] in the sense that all the 1-body and 2-body amplitudes are taken into account.

References

1. See references in "Time-Dependent Hartree-Fock and Beyond," vol. 171 of Lecture Notes in Physics, edited by K. Goeke and P.G. Reinhard (Springer, Berlin, 1982).

2. S.J. Wang and W. Cassing, Ann. Phys. 159, 328 (1985); W. Cassing and S.J. Wang, Z. Phys. A328, 423, (1987).

3. M. Tohyama and M. Gong, Z. Phys. A332, 269 (1989).

4. J. Sawicki, Phys. Rev. 126, 2231 (1962).

5. J. Da Providencia, Nucl. Phys. 61, 87 (1965).

6. C. Yannouleas, M. Dworzecka and J.J. Griffin, Nucl. Phys. A397, 239 (1983).

7. S. Ayik and M. Dworzecka, Phys. Rev. Lett. 54, 534 (1985).

Transverse Hydrodynamics of Collective Flow

D. Kusnezov and G. Bertsch

An interesting feature of the pion spectra observed in ultra-relativistic collisions is a low-transverse momentum peak, which is not found in the spectra from nucleon collisions. It has been suggested that the peak could be explained as an effect of hydrodynamics, the cooling of the pion gas as it expands. We have made some detailed hydrodynamic calculations and find that this explanation is untenable.

The basic ingredients of the calculation are the equation of state and the assumptions about the freezeout, i.e. the conditions at which the fluid is assumed to become the final state particle distribution. We assumed an ideal relativistic fluid, and that freezeout occurs in a fluid element when the temperature in that element reaches some value.

We considered a wide range of starting conditions. The initial hydrodynamics is started from matter at rest at times in the range 0.1 fm/c to 5 fm/c. The energy density at the freezeout surface was considered for a range of values going down to 1/1000 of the initial energy density. In all cases the transverse momentum distribution of the pions is nearly flat for momenta less than 100 fm/c, in contrast to the data (See Fig. 1).

The reason our results are at variance with the previous claims can be traced to the definition of the freezeout surface. If the freezeout is assumed to occur at a certain time in some global reference frame, the peak can be reproduced. However, on physical grounds, a local criterion for freezeout is called for, and then the freezeout surface is curved in such a way as to de-emphasize low-momentum particles.

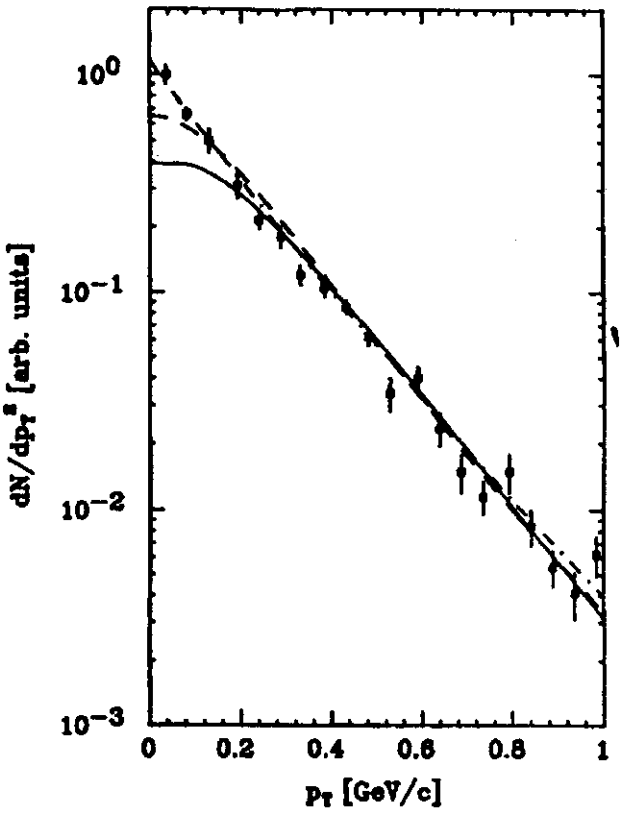

FIG. 1: Comparison of transverse momentum spectrum of pions in ultrarelativistic collisions to several models. The data points are from Ref. 1. The solid curve is representative of our calculations. The dashed curve is hydrodynamic with a freezeout at fixed global time. The dot-dash curve is the model of Ref. 2.

References

1. H. Stroebele *et al.*, Z. Phys. C38, 89 (1988).

2. T. W. Atwater, P.S. Freier and J. Kapusta, Phys. Lett. B199, 30 (1987).

Impact Parameter and Energy Dependence of Observables in Intermediate-Energy Heavy-Ion Reactions

M.B. Tsang, G. Bertsch, W. Lynch and M. Tohyama

To explore the properties of reaction filters for heavy-ion reactions at intermediate energy, we performed calculations with the Boltzmann equation[1] for several systems. We calculated experimental observables such as the linear and angular momentum transferred to the target residue, the multiplicities and momentum distributions of emitted nucleons, and properties of the projectile-like residues predicted in collisions at large impact parameter. Details of the calculations are given in Ref. 1.

A. ^{14}N + ^{154}Sm at E/A = 35 MeV

In this section we will discuss in detail the $^{14}N+^{154}Sm$ reaction at E/A = 35 MeV where our most extensive set of calculations were performed. Observables for this system were calculated at an elapsed time of 200 fm/c. The target residue velocity, V_r, is surprisingly insensitive to impact parameter for $b \leq 7$ fm. At large impact parameters, $b \geq 7$ fm, where projectile-like residues can be identified in the calculation, V_r drops off sharply with increasing impact parameters. For $b \leq 7$ fm, the calculations predict that the impact parameter dependence is reflected most clearly in the angular momentum of the reaction residue; this increases monotonically with b until $b \approx 6.5$ fm, then falls off rapidly at larger impact parameters.

Projectile-like fragments are observed at impact parameters larger than 7 fm. In Fig. 1, the mass, deflection angle, energy per nucleon of the projectile-like residue, and mean transverse momentum P_{xf}/A_f carried by a nucleon in the projectile-like residue, are plotted as solid points for values of the impact parameter greater than 7 fm. The open points are results calculated with a modified Boltzmann code, which includes both the Coulomb field for proton test particles and a density dependent symmetry potential.[2] The mass and velocity of the target-like residue parallel to the beam axis (not shown) are only slightly modified by the inclusion of the Coulomb mean field.

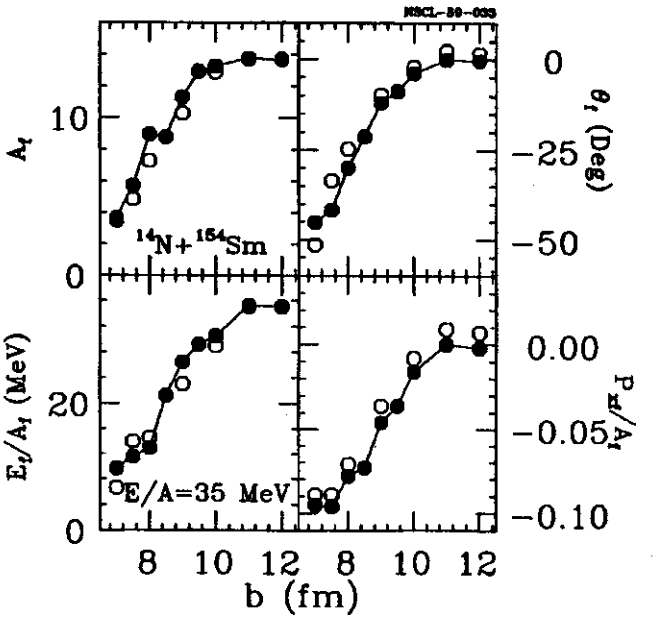

FIG. 1: Predictions for the mass (upper left), angle (upper right), energy per nucleon (lower left), and transverse momentum per nucleon (lower right) of the projectile-like residue for the $^{14}N+^{154}Sm$ reaction at E/A = 35 MeV. Calculations which include the Coulomb mean field are designated by the open points. Calculations which exclude the Coulomb mean field are designated by the closed points. The solid lines are drawn to guide the eye.

For calculations with and without the Coulomb mean field, all four properties of the projectile shown in Fig. 1 increase with impact parameter. Inclusion of the Coulomb mean field leads to a systematic decrease in the projectile-like residue mass, an increase in the deflection angle that is especially pronounced at impact parameters around 8 fm, and positive scattering angles at larger impact parameters, $b \geq 10$ fm. Since fluctuations are important to intermediate-mass fragment emission[3] but are strongly suppressed by the ensemble-averaging used in the computation of the mean field[3], the connection between the properties of the calculated fragments and the properties of experimentally observed fragments is somewhat tenuous.

The differential multiplicities for nucleons with laboratory energies greater than 5 MeV were also computed at each impact parameter and then integrated over laboratory

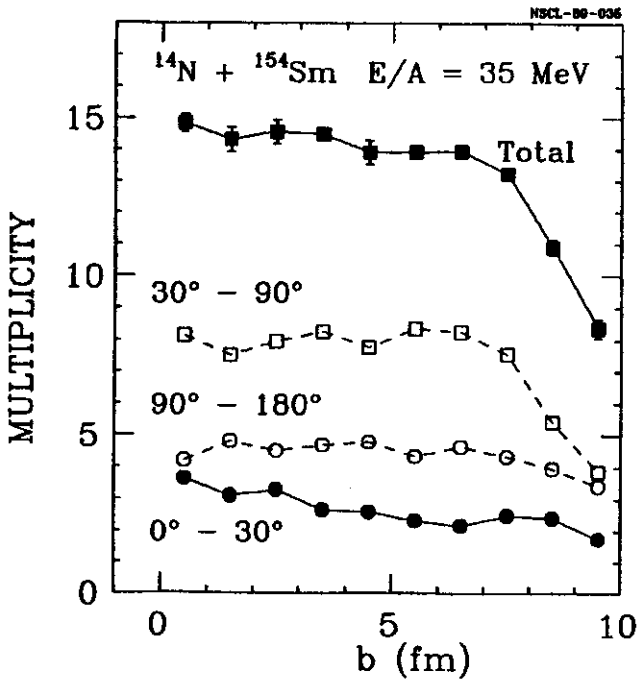

FIG. 2: Nucleon multiplicities for the $^{14}N+^{154}Sm$ reaction at E/A = 35 MeV are given by the solid and open points in the figure. These multiplicity distributions were integrated over the angular ranges indicated in the figure. Smaller uncertainties occur for points at impact parameters for which more than one calculation were performed. The lines are drawn to guide the eye.

angles for three angular ranges, 0°-30°, 30°-90°, and 90°-180°. The resulting nucleon multiplicities are shown in Fig. 2. At large impact parameters, the nucleon multiplicities drop steeply, with increasing impact parameters reflecting the decreased overlap of projectile and target. At smaller impact parameters, the nucleon multiplicities are remarkably insensitive to the impact parameter. When one also considers that statistical fluctuations will smear out the correlation between multiplicity and impact parameter, it is clear that the residue velocity provides a better indication of the impact parameter for this reaction. An even better measure of the impact parameter might be obtained if one could combine either measurement with a probe, like the γ-ray multiplicity, which is sensitive to the angular momentum transfer to the target-like residue.

Information about the reaction dynamics is also contained in the mean transverse momentum, $<P_x>$, as well as the emission pattern of unbound nucleons.[5] Solutions of the Boltzmann equation indicate that the mean transverse momentum in intermediate-energy heavy-ion collisions is very sensitive to the interplay between the attractive nuclear mean field and nucleon-nucleon collisions.[6] The mean transverse momentum of unbound nucleons is negative at all impact parameters for this reaction. The negative values for $<P_x>$ are consistent with experimental measurements of the circular polarization of γ-rays emitted by the target residue[7]; they suggest the dominance of the attractive nuclear mean field. The mean transverse momentum decreases with increasing impact parameter, until a minimum is reached at about 6 fm, then it increases and vanishes at much larger impact parameter. Such a strong impact parameter dependence clearly illustrates the need to develop a good experimental measure of the impact parameter.

The calculation indicates that nucleons are emitted preferentially in the reaction plane. Experimentally, such effects have been reported by Ref. 4. The preference for in-plane emission increases with the energy of the outgoing particle. Such an energy-dependent in-plane enhancement has been observed experimentally for the reaction of $^{14}N+^{157}Au$ at E/A = 30 MeV.[4] The experimental in-plane enhancement is also observed to increase strongly with the mass of the detected particle.[4] Unfortunately, any mass dependence of the emitted particles cannot be studied in the present model without invoking additional assumptions about the fragment production mechanism. Since these uncertainties in the fragment production mechanism have a significant influence on the in-plane enhancement of particle emission patterns, we have not attempted to determine the sensitivity of the different observables to the azimuthal orientation of the reaction plane.

To explore the sensitivity of these predictions to the nucleon-nucleon cross section, additional calculations were performed with a reduced nucleon-nucleon cross section of $4\pi\sigma_{nn}=20$ mb. The nucleon distributions are slightly more forward-peaked and more enhanced in the reaction plane in calculations where the nucleon-nucleon cross section is reduced. The mean transverse momenta shown in Fig. 3 are significantly more negative.[7] These differences are not unexpected, since nucleon-nucleon collisions make the nucleon velocity distributions for this bombarding energy

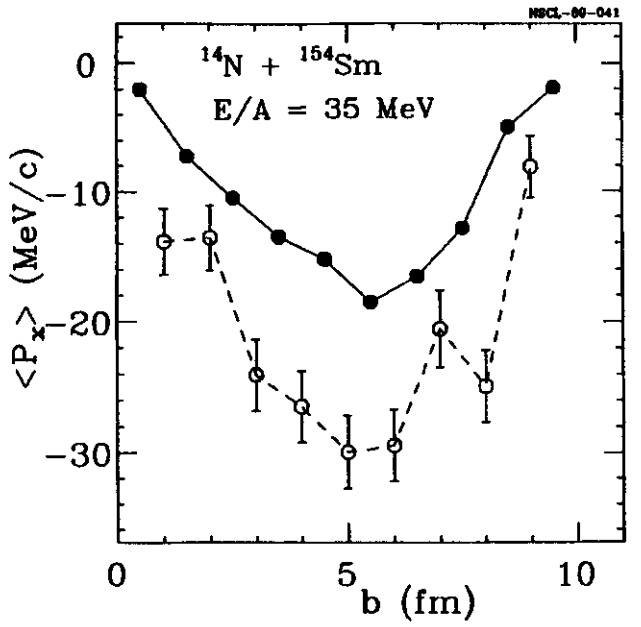

FIG. 3: Values for the mean transverse momentum of unbound nucleons calculated with the Boltzman equation and a nucleon-nucleon cross section 41 mb are plotted here as solid points for ^{14}N+^{154}Sm reactions at E/A=35 MeV. The corresponding calculations with a reduced nucleon-nucleon cross section of 20 mb are given by the open points. Statistical uncertainties for both calculations are about the same. The lines are drawn to guide the eye.

domain more random and isotropic. The overall nucleon multiplicity is also somewhat lower with the reduced nucleon-nucleon cross section and is more sensitive to impact parameter. The velocity of the heavy residue is also somewhat less.

In principle, these differences may enable one to determine empirically the most appropriate nucleon-nucleon cross section for these simulations. The strongest sensitivities to the nucleon-nucleon cross section are displayed by the mean transverse momenta and the in-plane enhancement of the nucleon emission patterns. These two observables, however, are strongly impact parameter-dependent, illustrating the importance of establishing reliable measures of the impact parameter.

B. The Bombarding Energy Dependence of the Nucleon Multiplicities

As the bombarding energy is increased, it becomes increasingly advantageous to be able to select the impact parameter using the properties of the unbound nucleons or light particles. To illustrate the evolution of the nucleon multiplicity distributions with impact parameter, we have calculated the nucleon multiplicity distributions for the symmetric ^{40}Ar+^{40}Ar system and the mass asymmetric ^{16}O+^{197}Au system for E/A between 35 and 400 MeV.

We consider first calculations for the ^{40}Ar+^{40}Ar system. In these calculations, nucleon multiplicities were evaluated after an elapsed time of 200, 150, 100, 75, and 50 fm/c for calculations performed at the incident energies E/A=35, 60, 100, 200, and 400 MeV, respectively. Fusion is predicted to occur only at $b=1$ fm for collisions at E/A=35 MeV. At this energy and larger impact parameters, well formed projectile- and target-like residues can be identified at the end of each calculation. At higher energies, two bound residues occur mainly at large impact parameters; at small impact parameters, many fragments are frequently produced.

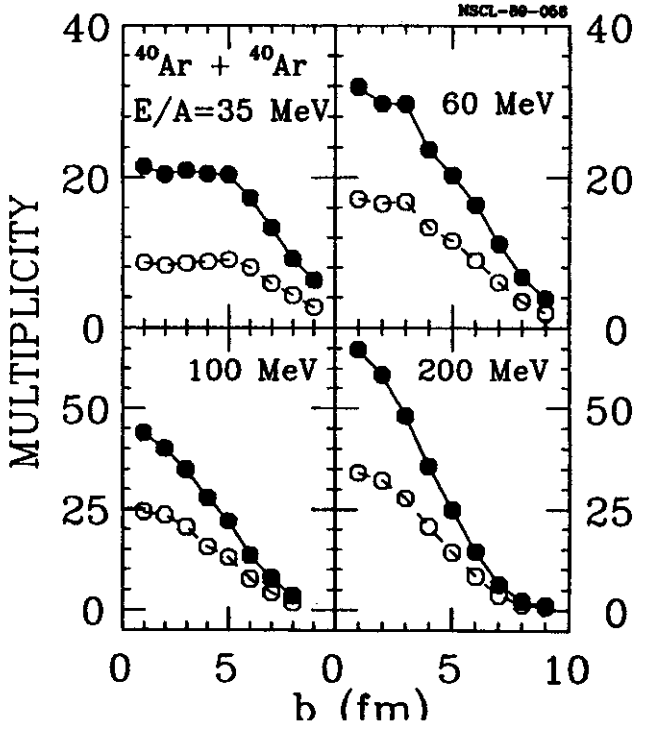

FIG. 4: Total nucleon multiplicities are given by the solid points and the multiplicity of nucleons at $\theta<30°$ by the open points for the ^{40}Ar+^{40}Ar reaction at bombarding energies of E/A=35, 60, 100 and 200 MeV. The lines are drawn to guide the eye.

The total multiplicity and the multiplicity of nucleons emitted at $\theta_{lab} \leq 30°$ are shown in Fig. 4 for the ^{40}Ar+^{40}Ar system at four bombarding energies. Like the ^{14}N+^{154}Sm system at E/A=35 MeV, the total multiplicity for the

$^{40}Ar+^{40}Ar$ system at E/A=35 MeV is insensitive to impact parameter for small impact parameters. At higher energies, however, the total multiplicity displays a monotonic, almost linear, dependence on impact parameter. The multiplicity at any given impact parameter grows with incident energy and reaches limiting values consistent with the participant spectator model by E/A=200 MeV. Multiplicities calculated at E/A=400 MeV (not shown) are about 10% larger and have essentially the same dependence on impact parameter as those calculated at E/A=200 MeV.

The energy dependence of the multiplicity distributions for $^{16}O+^{197}Au$ reactions is shown in Fig. 5. It is interesting to note that the impact parameter dependences of both the calculations at E/A=200 and 400 MeV are qualitatively similar to those displayed for the $^{16}O+^{197}Au$ reaction at E/A=90 MeV. Such dependences are different from those predicted for collisions between mass-asymmetric systems at lower energies. By combining information provided by the total multiplicity and the forward angle multiplicity, these calculations suggest that multiplicity measurements may provide more quantitative impact parameter information at small impact parameters for collisions at and above E/A≈90 MeV than below.

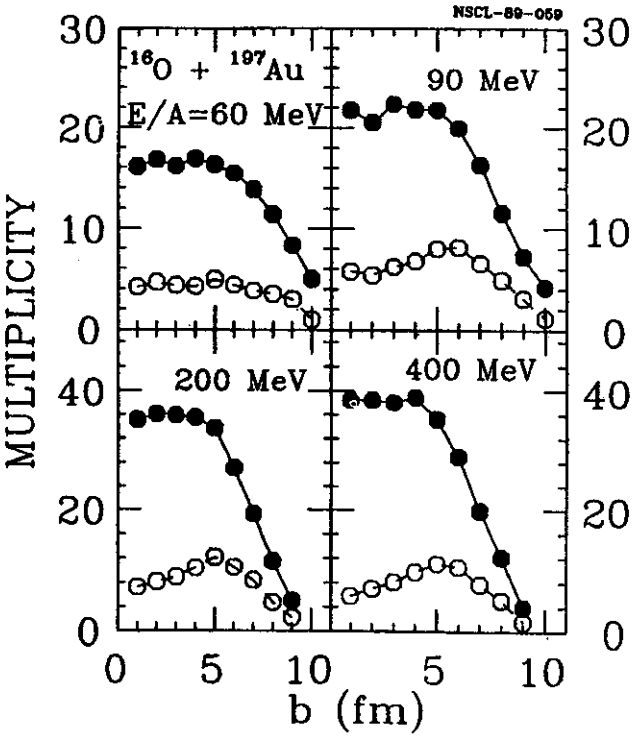

FIG. 5: Total nucleon multiplicities are given by the solid points and the multiplicity of nucleons at $\theta < 30°$ by the open points for the $^{16}O+^{197}Au$ reaction at bombarding energies of E/A = 60, 90, 200 and 400 MeV. These multiplicity distributions were integrated over the angular ranges indicated in the figure. The lines are drawn to guide the eye.

References

1. J. Aichelin and G. Bertsch, Phys. Rev. C31, 1730 (1985).

2. M. Betty Tsang, George F. Bertsch, William G. Lynch, M. Tohyama, MSU preprint MSUCL- 681.

3. W. Bauer G.F. Bertsch and S. Das Gupta, Phys. Rev. Lett. 58, 863 (1987).

4. M.B. Tsang *et al.*, Phys. Rev. Lett. 52, 1967 (1984).

5. P. Danielewicz, and G. Odyniec, Phys. Lett. B157, 146 (1985).

6. G.F. Bertsch, W.G. Lynch and M.B. Tsang, Phys. Lett. B189, 384 (1987).

7. M.B. Tsang *et al.*, Phys. Rev. Lett. 57, 559 (1986).